Effect of Ru Species on N$_2$O Decomposition over Ru/Al$_2$O$_3$ Catalysts

Chao Sui [1], Fulong Yuan [1], Zhiping Zhang [1], Chi Zhang [1], Xiaoyu Niu [1,2,*] and Yujun Zhu [1,*]

[1] Key Laboratory of Functional Inorganic Material Chemistry (Heilongjiang University), Ministry of Education, School of Chemistry and Materials, Heilongjiang University, Harbin 150080, China; suichao071@163.com (C.S.); fulongyuan2000@yahoo.com (F.Y.); baiheboshi@163.com (Z.Z.); zlc018018@126.com (C.Z.)

[2] College of Environmental and Chemical Engineering, Heilongjiang University of Science and Technology, Harbin 150022, China

* Correspondence: niuxiaoyu2000@126.com (X.N.); yujunzhu@hlju.edu.cn (Y.Z.); Tel.: +86-451-86609650 (X.N. & Y.Z.)

Abstract: Ru is considered as an effective active species for N$_2$O decomposition; however, there is disagreement about which ruthenium species is key for catalytic activity. In order to understand the role of Ru species in N$_2$O decomposition, Ru/Al$_2$O$_3$ (Ru/Al$_2$O$_3$-H$_2$, Ru/Al$_2$O$_3$-NaBH$_4$, Ru/Al$_2$O$_3$-air) catalysts with different ratios of metallic Ru were prepared and evaluated for their catalytic activities. Various characterizations, especially in situ diffuse reflectance infrared Fourier transform spectroscopy (DRIFTS), were applied to investigate the relationship between activity and different Ru species. The results indicate that the N$_2$O conversion displayed a linear relationship with the amount of metallic Ru. The DRIFTS results of adsorption for N$_2$O show that metallic Ru was the active site. The catalytic processes are put forward based on metallic Ru species. The deactivation with increasing times used is due to the decrease in the amount of metallic Ru and agglomerates of Ru particles on the surface of catalysts.

Keywords: N$_2$O decomposition; metallic Ru; deactivation reason

1. Introduction

In recent years, N$_2$O has become one of the major pollutants for the destruction of ozone in the stratosphere and a mighty greenhouse gas because of its long life time (110–150 years) in the atmosphere and its 310-times higher greenhouse potential than CO$_2$ [1–5]. Now, N$_2$O atmospheric concentration is growing at a rate of about 0.5–1.0 ppbv (parts per billion by volume) per year as a consequence of anthropogenic activities, including the combustion of fossil fuels and biomass and the production of adipic and nitric acid in chemical plants [6]. Therefore, N$_2$O abatement is realized by control of N$_2$O emissions with end-of-pipe technologies from combustion and chemical processes. The catalytic decomposition of N$_2$O into N$_2$ and O$_2$ is a very efficient and economical way to reduce its negative environmental impact [7].

In recent years, many of the catalysts have been studied for the N$_2$O decomposition reaction, including noble metal (Au, Ru, Rh, Pd, Pt, Ir) and non-noble metal (Fe, Cu, Co, Ni) on a variety of supports, such as perovskites, metal oxides (Al$_2$O$_3$, SiO$_2$, CaO, TiO$_2$, CeO$_2$, Fe$_2$O$_3$), hydrotalcites, zeolites (ZSM-5, BEA, USY, ferrierite) and mesoporous materials (MCM-41, SBA-15) [8–22]. Li et al. [23] investigated the M/ZSM-5 catalysts and found that the catalytic activity for N$_2$O decomposition followed the order: Ru, Rh > Pd > Cu > Fe > Pt > Ni > Mn. Meanwhile, Ru was considered as having one of the best activities among these metals.

Ru is an effective catalyst for N–O bond dissociation, so that it promotes N_2O decomposition [24–27]. Benco's [14] report confirmed the activation of the N_2O molecule by calculation using DFT over Ru. It was found that the activation energy of Ru was much lower than that of Co and Fe. Kawi et al. [28] investigated Ru on the MCM-41, showing far high activity for N_2O decomposition, and N_2O conversion reached 100% at 400 °C. The catalytic activity of Ru metal was influenced by size, support, interaction and O_2. Komvokis et al. [13] reported that Ru formed with sizes from 1–3 nm with high dispersion (70%), which showed much higher catalytic activity and stability for N_2O decomposition. In the case of Rh catalysts [29], Rh/MgO, Rh/SiO_2 with Rh sizes of 2.1–2.4 nm were more active than Rh/CeO_2, Rh/Al_2O_3 and Rh/TiO_2 with small particles of 1.0–1.4 nm for the N_2O decomposition. For different supports [30], the strength of interaction between Ru and support was concluded to be $MgO > TiO_2 > Al_2O_3 = SiO_2$. However, catalytic activity was as follows: $Ru/TiO_2 > Ru/Al_2O_3 > Ru/SiO_2 > Ru/MgO$. Besides, the reducibility of the Ru metal particle was found to be a crucial factor. Komvokis reported that the catalytic activity of N_2O decomposition was much higher by H_2-pretreated catalyst (metallic Ru) because of the cyclic oxidation-reduction pathway of metallic Ru [31]. It was well known that desorption of O_2 represents the rate-determining step in N_2O decomposition. The presence of O_2 has an inhibitory effect on the N_2O decomposition and decreases reaction rates over supported noble metal catalysts [32]. Zhang et al. [30] reported that the sensitivity of noble metal to O_2 in feed gas was dependent on the reducibility of support material. It was concluded to be $Ru/SiO_2 > Ru/Al_2O_3 > Ru/TiO_2 > Ru/CeO_2$.

In fact, the catalytic performance and deactivation of supported Ru catalysts is still a complex issue for N_2O decomposition. In the present study, a series of Ru/Al_2O_3 catalysts as model catalysts is prepared by using different pretreatment methods, and their catalytic activity and stability in the decomposition of N_2O were investigated. Furthermore, the change of Ru species and the deactivation factor were suggested by combining various characterizations, including XPS, TEM, in situ diffuse reflectance infrared Fourier transform spectroscopy (DRIFTS), Temperature- programmed desorption of N_2O (N_2O-TPD), etc. Meanwhile, we put forward the reaction process of N_2O decomposition over Ru on the surface of Ru/Al_2O_3 catalysts.

2. Results

2.1. Characterization of Prepared Samples

The Ru/Al_2O_3, the five-times used Ru/Al_2O_3 (after using Ru/Al_2O_3 five-times) and Al_2O_3 samples were studied by XRD in Figure 1. All of the reflections of the Ru/Al_2O_3 and five-times used Ru/Al_2O_3 catalysts present in the diffractogram match well with the cubic spinel structure of γ-Al_2O_3 (JCPDS PDF No. 10-0425) [33]. It was observed that neither metallic Ru nor RuO_x species could be identified in the patterns of Ru/Al_2O_3 and five-times used Ru/Al_2O_3 catalysts, which indicated that ruthenium was represented by the mean of the high dispersion in these samples.
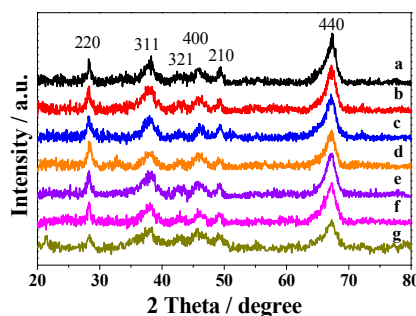
Figure 1. XRD patterns of: (**a**) Al_2O_3; (**b**) Ru/Al_2O_3-H_2; (**c**) Ru/Al_2O_3-$NaBH_4$; (**d**) Ru/Al_2O_3-air; (**e**) five-times used Ru/Al_2O_3-H_2; (**f**) five-times used Ru/Al_2O_3-$NaBH_4$; (**g**) five-times used Ru/Al_2O_3-air catalysts.

TEM analysis was carried out over fresh (a–c) and five-times used (d–f) Ru/Al_2O_3-$NaBH_4$ catalysts shown in Figure 2. It can be seen that the Ru particle was not observed in fresh Ru/Al_2O_3-$NaBH_4$ samples, which should be due to the much smaller particle size of Ru (less than 1 nm). However, the five-times used Ru/Al_2O_3-$NaBH_4$ catalyst was found to have agglomerates of Ru particles. The particles had an average size of about 5–20 nm, while particles with a size up to 40 nm could also be found. The HRTEM image shows that the distance of two adjacent planes of the selected particle is about 0.203 nm, which is corresponding to the (101) lattice plane of the metal Ru.
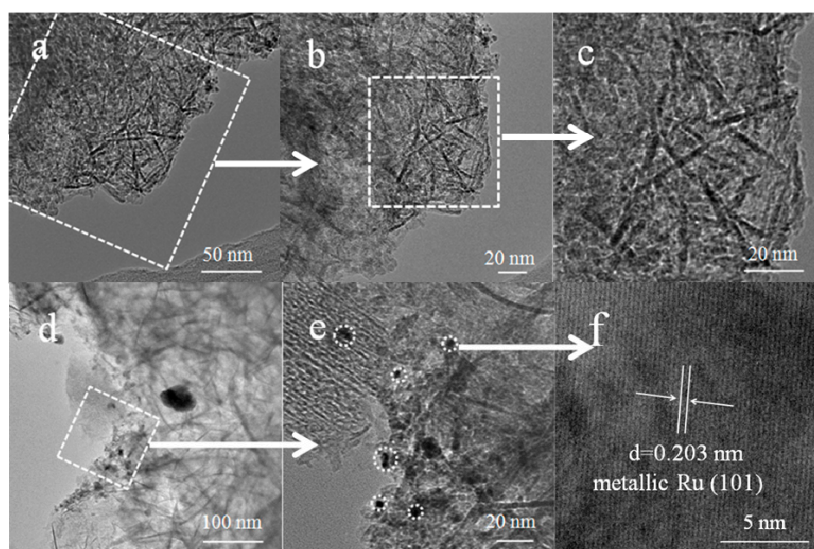
Figure 2. TEM profiles of fresh Ru/Al_2O_3 (**a**–**c**) and five-times used Ru/Al_2O_3 (**d**–**f**).

In order to confirm the actual content of Ru, the chemical analysis (ICP-AES) was tested. It showed that the Ru content was 0.50 ± 0.02 wt % for the Ru/Al_2O_3 and used Ru/Al_2O_3 catalysts, which was close to the theoretical content (0.50 wt %) in Table 1. The BET surface area of Ru/Al_2O_3, used Ru/Al_2O_3 and Al_2O_3 are summarized in Table 1. The surface areas of Ru/Al_2O_3 and used Ru/Al_2O_3 catalysts were almost close to 196–201 m^2/g, which were slightly lower than those of Al_2O_3 catalyst (204 m^2/g).

Table 1. Physicochemical properties of the catalysts.

Catalysts	Surface Area (m^2/g)	Metallic Ru (eV) [a]		Ru^{4+} (eV) [a]		Metallic Ru/Ru^{4+} (%) [b]
		$3d_{5/2}$	$3d_{3/2}$	$3d_{5/2}$	$3d_{3/2}$	
Al_2O_3	204	-	-	-	-	-
Ru/Al_2O_3-H_2	199	279.8	284.0	285.0	289.0	60/40
1-time used Ru/Al_2O_3-H_2	196	280.4	284.5	285.6	288.5	38/62
5-times used Ru/Al_2O_3-H_2	196	280.4	284.3	285.0	288.0	26/74
Ru/Al_2O_3-$NaBH_4$	201	280.0	284.1	285.0	289.1	51/49
1-time used Ru/Al_2O_3-$NaBH_4$	199	278.8	283.0	284.0	288.0	47/53
5-times used Ru/Al_2O_3-$NaBH_4$	199	280.0	284.0	285.0	288.7	15/85
Ru/Al_2O_3-air	200	280.0	284.0	285.0	289.0	29/71
1-time used Ru/Al_2O_3-air	196	280.0	283.5	285.3	289.3	21/80
5-times used Ru/Al_2O_3-air	196	280.5	284.6	285.2	288.6	8/92
used Ru/Al_2O_3-$NaBH_4$ (cool under He)	-	280.0	283.7	285.8	288.0	40/60

[a] Peaks were attributed to the $3d_{5/2}$ and $3d_{3/2}$ of metallic Ru and Ru^{4+} species; [b] the relative amounts of metallic Ru and Ru^{4+} species were calculated from the areas of the fitted Gaussian–Lorentzian components of Ru3d.

To better understand the chemical state of Ru on the catalysts surface, the Ru/Al_2O_3 catalysts were investigated by the XPS technique. Figure 3 presents the XPS and the peak fitting results of Ru3d for the fresh and used Ru/Al_2O_3-H_2, Ru/Al_2O_3-$NaBH_4$ and Ru/Al_2O_3-air catalysts. The peaks at 280.2 and

285.0 eV were attributed to the $3d_{5/2}$ of metallic Ru and Ru^{4+} species, respectively, and corresponding to the $3d_{3/2}$ binding energies at 284.4 (metallic Ru) and 289.1 eV (Ru^{4+}) [34,35]. The relative amounts of metallic Ru and Ru^{4+} species were calculated from the areas of the fitted Gaussian–Lorentzian components of Ru3d shown in Table 1. It was noteworthy that the number of metallic Ru species was different on the surface of theses catalysts. The amount of the metallic Ru was about 60%, 51% and 29% for the Ru/Al_2O_3-H_2, Ru/Al_2O_3-$NaBH_4$ and Ru/Al_2O_3-air, respectively. To determine the change of Ru chemical state and surface composition, XPS studies were also carried out over the used Ru/Al_2O_3 catalysts. The amount of the metallic Ru was about 38% and 26% for one-time used Ru/Al_2O_3-H_2 and five-times used Ru/Al_2O_3-H_2, respectively, which indicated that the number of metallic Ru species on the surface of used Ru/Al_2O_3-H_2 catalyst was less than that of the fresh catalyst (Table 1); moreover, it gradually decreased with the increase in times used. Similarly, the amount of metallic Ru species also decreased with the repeated times used for Ru/Al_2O_3-$NaBH_4$ (51%, 47% and 15% for fresh, one-time used time and five-times used times) and Ru/Al_2O_3-air catalysts (29%, 21% and 8% for fresh, one-time used time and five-times used times). The above results reveal that the Ru/Al_2O_3 catalysts present different Ru species (metallic Ru and Ru^{4+}), and the valence state of the Ru species increased with use time.
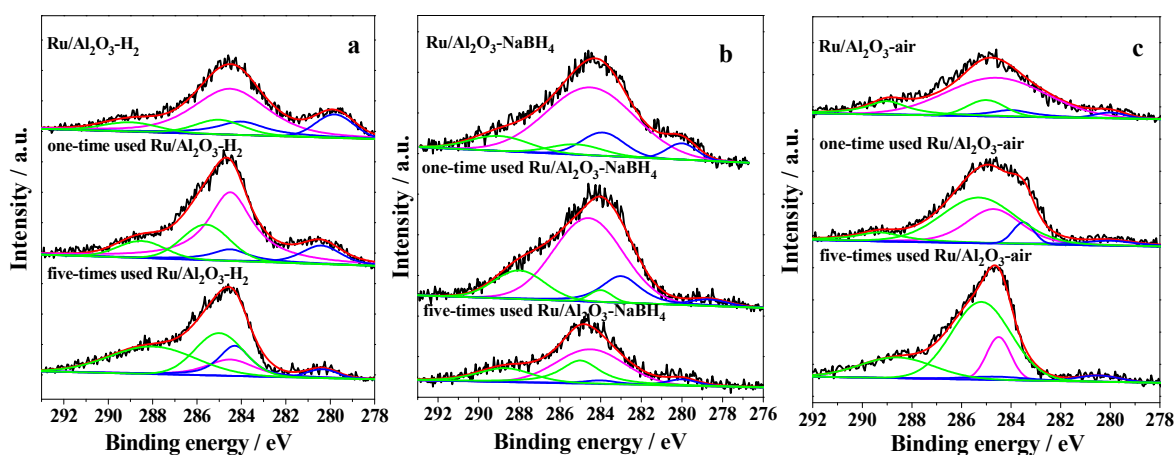
Figure 3. XPS of Ru3d for fresh and used (**a**) Ru/Al_2O_3-H_2; (**b**) Ru/Al_2O_3-$NaBH_4$; (**c**) Ru/Al_2O_3-air catalysts (black line: original data line; red line: fitting curve; pink line: the characteristic peak of C; blue line: the characteristic peak of metallic Ru; green line: the characteristic peak of Ru^{4+}).

2.2. Catalytic Activity Studies

Figure 4 shows the dependence of N_2O conversion on the reaction temperature from 250 °C–450 °C in direct N_2O decomposition over the Ru/Al_2O_3 and Al_2O_3 catalysts. As shown in Figure 4, there was no activity for N_2O decomposition over Al_2O_3 in the tested temperature range. N_2O conversion was below 40% at 350 °C over the Ru/Al_2O_3-air; meanwhile, Ru/Al_2O_3-$NaBH_4$ and Ru/Al_2O_3-H_2 catalysts exhibited above 48% and nearly 62% conversion of N_2O at 350 °C, respectively. In Figure 4, it was obvious that the catalytic activity was different below 400 °C among the Ru/Al_2O_3 catalysts, and the order of N_2O conversion was followed as: Ru/Al_2O_3-H_2 > Ru/Al_2O_3-$NaBH_4$ > Ru/Al_2O_3-air > Al_2O_3. However, it can be clearly seen that the difference in the catalytic activities was smaller and smaller with the increase in reaction temperature above 375 °C among the Ru/Al_2O_3-H_2, Ru/Al_2O_3-$NaBH_4$ and Ru/Al_2O_3-air catalysts, and the N_2O conversions were nearly 95% over these catalysts at 425 °C. In the literature [13,27,30,31,36–40], the catalytic activity of catalysts was different for N_2O decomposition, as shown in Table S1. Ru/r-TiO_2 exhibited better activity than our prepared catalysts; however, the Ru content in Ru/r-TiO_2 was far higher than 0.5%. The temperature of 50% conversion to N_2O for Ru/Al_2O_3 was lower than that for other Ru-based catalysts. Compared

with other catalysts (Rh, Pt, Pd, Ir), the catalytic activity of Ru/Al_2O_3 was higher at almost the same gas hourly space velocity (GHSV).
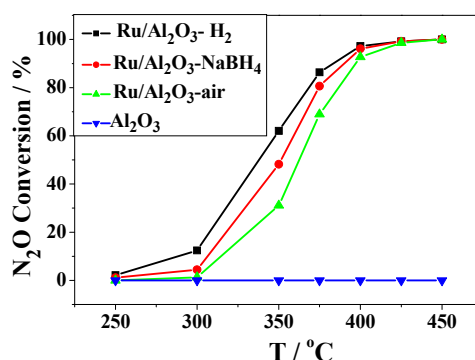
Figure 4. N_2O conversion as a function of reaction temperature over fresh Ru/Al_2O_3 catalysts (reaction condition: $[N_2O]$ = 5000 ppm and gas hourly space velocity (GHSV) = 11,000 h^{-1}).

To confirm the repeated practicability of the catalyst, each of the Ru/Al_2O_3-H_2, Ru/Al_2O_3-$NaBH_4$ and Ru/Al_2O_3-air catalysts was tested continually repeating five-times from 250 °C–475 °C. Figure 5 shows the N_2O conversion for each of fresh and used Ru/Al_2O_3 catalysts. In Figure 5a, the Ru/Al_2O_3-H_2 catalyst exhibited instable activity that decreased with increasing used times. Obviously, the phenomenon was found that the N_2O conversion decreased from 250 °C–400 °C and dropped from 86% down to 66% at 375 °C after using 5 times. In Figure 5b,c, the Ru/Al_2O_3-$NaBH_4$ and Ru/Al_2O_3-air catalysts also show deactivation with the repeated use, and the N_2O conversion dropped from 81% down to 41% and 69% down to 45% at 375 °C after using five times, respectively. It was concluded that the catalytic activities of the Ru/Al_2O_3 catalysts were different and decreased with the increase in the evaluated times.
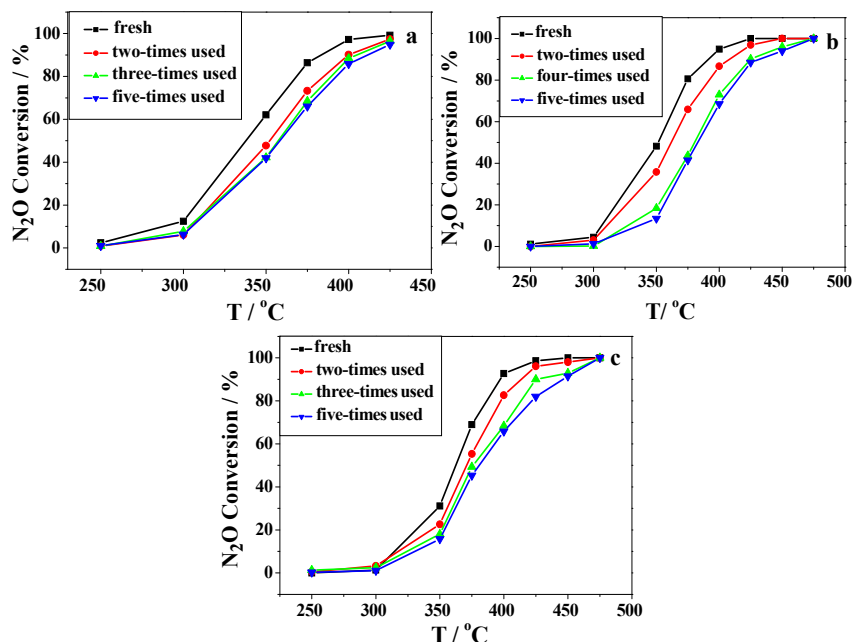
Figure 5. N_2O conversion as a function of reaction temperature over: (**a**) Ru/Al_2O_3-H_2; (**b**) Ru/Al_2O_3-$NaBH_4$; (**c**) Ru/Al_2O_3-air catalysts (reaction condition: $[N_2O]$ = 5000 ppm and gas hourly space velocity (GHSV) = 11,000 h^{-1}).

It is possible that there are some certain relationships between the N_2O conversion and the amount of surface metallic Ru. As shown in Figure 6, N_2O conversion increased with the amount of metallic Ru, which demonstrates that metallic Ru plays a key role in the conversion of N_2O. Furthermore, it can be clearly seen that there was no obvious difference in the N_2O conversion with the increase in the amount of metallic Ru at high temperature (above 425 °C), which was due to a high reaction rate. On the whole, the metallic Ru is the active site in the catalytic decomposition of N_2O.
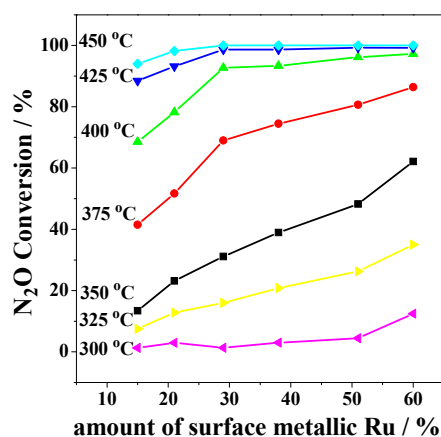
Figure 6. Relationship between N_2O conversion and the amount of surface metallic Ru.

The effect of time-on-stream on activity was also tested over the catalyst. Figure 7 shows the N_2O conversion versus time-on-stream curves for Ru/Al_2O_3-$NaBH_4$ catalyst. It can be seen that N_2O conversion was 100% and did not decrease for 700 min at 450 °C. After decreasing the reaction temperature to 20 °C and then increasing to 450 °C, the N_2O conversion did not change and was also 100%. It was noticed that the N_2O conversion was about 80% and slightly increased for 700 min at 375 °C. However, the deactivation phenomenon was found that the N_2O conversion dropped to 65% when the temperature was reduced to 20 °C and then increased to 375 °C. Then, the N_2O conversion slightly increased with the increase in reaction time. Nonetheless, it was less than that of before 700 min. The Ru/Al_2O_3 catalyst could maintain stable activity during the evaluated time. However, the catalytic activities of used Ru/Al_2O_3 catalysts decreased with the increase in the times used. This is consistent with Figure 5.
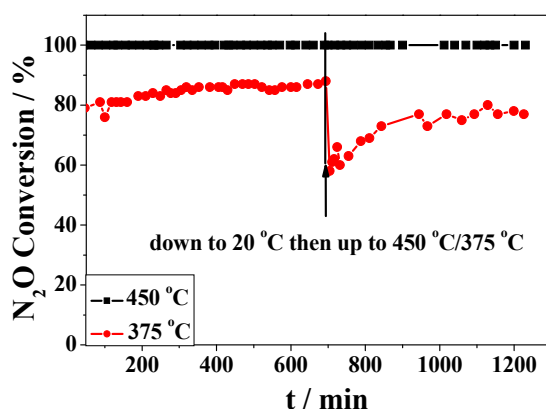
Figure 7. N_2O conversion versus time-on-stream over Ru/Al_2O_3-$NaBH_4$ catalyst (reaction condition: $[N_2O]$ = 5000 ppm and gas hourly space velocity (GHSV) = 11,000 h^{-1}).

Effects of gas hourly space velocity (GHSV) on the catalytic activity examined for the Ru/Al_2O_3 catalysts are displayed in Figure 8. It is clear that the temperature slightly shifted to a higher value for

the same N_2O conversion with increasing GHSV from 11,000–44,000 h^{-1}. The difference of temperature at a 50% conversion of N_2O is about 25 °C for GHSV 11,000 and 44,000 h^{-1}, which indicates that Ru/Al_2O_3 catalysts can be operated at a relative high GHSV.
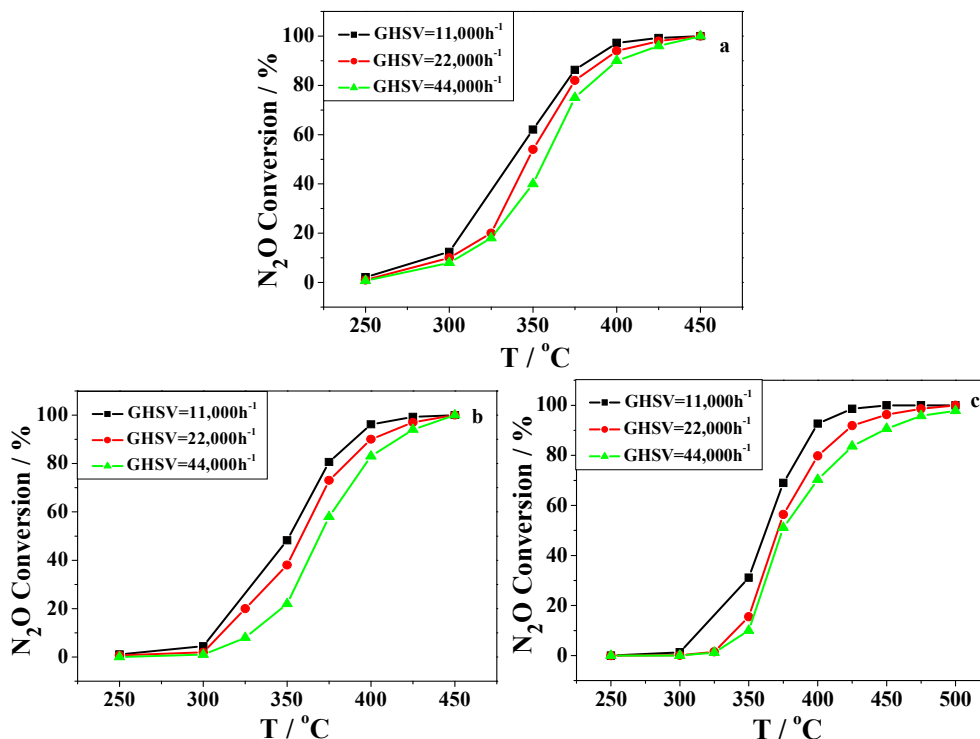
Figure 8. Effect of GHSV on the activity over (**a**) Ru/Al_2O_3-H_2, (**b**) Ru/Al_2O_3-$NaBH_4$ and (**c**) Ru/Al_2O_3-air catalysts (reaction conditions: 5000 ppm N_2O).

2.3. DRIFTS Studies

The N_2O adsorption on the Ru/Al_2O_3 catalysts had been studied by in situ DRIFTS in order to recognize the adsorbed species. Figure 9 shows the DRIFTS recorded with the support Al_2O_3 and Ru/Al_2O_3 under N_2O atmospheres. Generally, the N–N stretching frequency of adsorbed N_2O on metal oxides was reported within a wide range of frequencies between 2400 and 2150 cm^{-1}, and typical bands of the nitrites, nitrates and nitro species were located below 1700 cm^{-1} [41–45]. In Figure 9a, two quite intense absorption bands were observed at 2237 and 2212 cm^{-1}, which could be assigned to the N–N stretching of adsorbed N_2O [46]. The spectra of N_2O adsorption over Al_2O_3 support under N_2O flow showed some bands at 1300–1700 cm^{-1} that was assigned to monodentate nitrites, monodentate nitrates and nitro species, implying that the N_2O can adsorbed on the surface of the support Al_2O_3 [45]. Figure 9b shows the DRIFTS of adsorbed N_2O over Ru/Al_2O_3-$NaBH_4$. Four intense peaks at 1871, 1650, 1533 and 1410 cm^{-1} were observed along with characteristic peaks of gas-phase N_2O at 2237 and 2212 cm^{-1}. The bands at 1650, 1533 and 1410 cm^{-1} can be assigned to nitrate and nitrite species, monodentate nitrate species and nitro species, respectively [41–48]. The band at 1871 cm^{-1} can be attributed to the Ru–ON species [49]. Figure 9c,d show the DRIFTS of adsorbed N_2O over Ru/Al_2O_3-H_2 and Ru/Al_2O_3-air. The gas-phase N_2O, nitrate and nitrite species were also observed over Ru/Al_2O_3-H_2 and Ru/Al_2O_3-air catalysts. Simultaneously, the peak assigned to Ru–ON was detected at 1871 cm^{-1} over Ru/Al_2O_3-H_2; however, the corresponding peak was not found over Ru/Al_2O_3-air. This result should be due to the amount of metallic Ru on the surface of Ru/Al_2O_3-air catalyst being much less than that of Ru/Al_2O_3-H_2 and Ru/Al_2O_3-$NaBH_4$. The XPS results in Table 1 show that the amount of metallic Ru species is 60%, 51% and 29% for Ru/Al_2O_3-H_2, Ru/Al_2O_3-$NaBH_4$ and Ru/Al_2O_3-air, respectively. A much lower amount of metallic Ru leading to the formation of

Ru–ON species was on the surface of Ru/Al$_2$O$_3$-air. Therefore, the amount of Ru–ON species was so small that the peak did not form in Figure 9d.
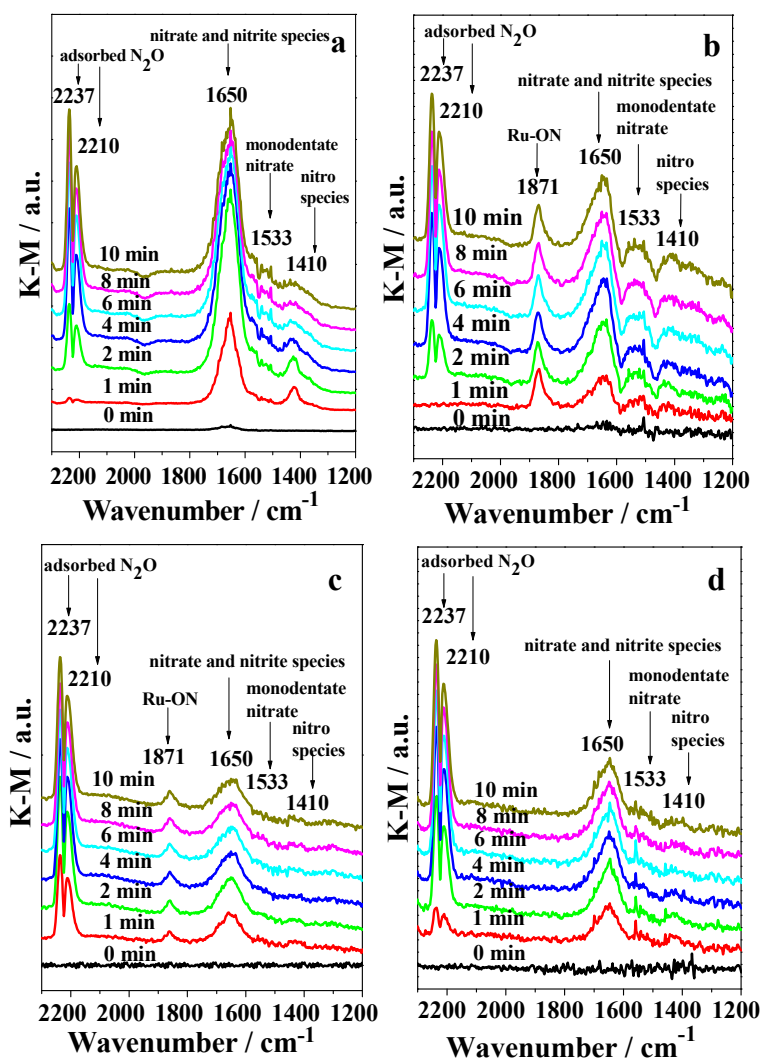
Figure 9. DRIFTS of N$_2$O adsorption on: (**a**) Al$_2$O$_3$; (**b**) Ru/Al$_2$O$_3$-NaBH$_4$; (**c**) Ru/Al$_2$O$_3$-H$_2$; (**d**) Ru/Al$_2$O$_3$-air at 50 °C. Condition: [N$_2$O] = 5000 ppm.

In order to understand the reaction process, DRIFTS studies have been carried out under flowing N$_2$O from 50 °C–375 °C over the Ru/Al$_2$O$_3$ catalysts displayed in Figure 10. In Figure 10a, the peak at 1650 cm^{-1} gradually disappeared from 50 °C–200 °C, which indicates the nitrate or nitrite species can easily decompose at a low temperature over the Ru/Al$_2$O$_3$-NaBH$_4$ catalyst. At the same time, the Ru–ON peak was clearly visible in the range of experimental temperatures. It was noted that the peak intensity of Ru–ON species increased by degrees from 50 °C–200 °C, which may be attributed to the amount of N$_2$O adsorption increasing on the surface of the catalyst and the formation of more Ru–ON species with increasing temperature. However, it became weak in the range of 250–375 °C, which should be related to the transformation or decomposition of Ru–ON species above 250 °C. It was found that N$_2$O decomposition occurred from 250 °C in Figure 4. Meanwhile, the intensity of the peak at 1533 cm^{-1} started increasing above 100 °C, which was due to the formation of the monodentate nitrates species on the surface of Ru/Al$_2$O$_3$-NaBH$_4$, and it was difficult to be decomposed and desorbed (Figure 10a). Figure 10b,c shows the DRIFTS of N$_2$O during temperature ramping on Ru/Al$_2$O$_3$-H$_2$ and Ru/Al$_2$O$_3$-air. The change of nitrate or nitrite specie (1650 cm^{-1}) species and monodentate nitrates

(1533 cm^{-1}) with increasing temperature was similar to that of Ru/Al$_2$O$_3$-NaBH$_4$. However, it was noteworthy that the peak assigned to the Ru–ON species at 1871 cm^{-1} almost disappeared above 250 °C for Ru/Al$_2$O$_3$-H$_2$, which is different with the Ru/Al$_2$O$_3$-NaBH$_4$. Combined with the XPS results, it is found that the amount of metallic Ru species decreases quickly to 38% from 60% after the first use for Ru/Al$_2$O$_3$-H$_2$, while it only reduced 4% (from 51% down to 47%) for Ru/Al$_2$O$_3$-NaBH$_4$ in this process. It is obvious to find the existence of more metallic Ru species on the surface of one-time used Ru/Al$_2$O$_3$-NaBH$_4$ compared with one-time used Ru/Al$_2$O$_3$-H$_2$, which is the advantage of the formation of Ru–ON species. Therefore, these results also confirm that the Ru–ON species is formed on the surface of the metallic Ru species of the Ru/Al$_2$O$_3$ catalysts.
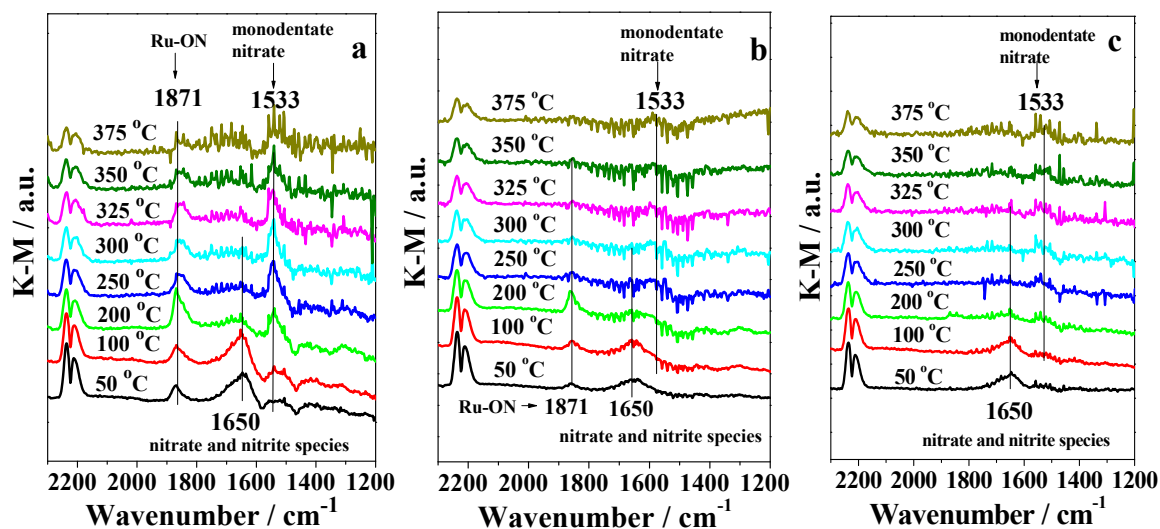
Figure 10. DRIFTS of 0.5% N$_2$O during temperature ramping on: (**a**) Ru/Al$_2$O$_3$-NaBH$_4$; (**b**) Ru/Al$_2$O$_3$-H$_2$; (**c**) Ru/Al$_2$O$_3$-air. Condition: [N$_2$O] = 5000 ppm.

The oxygen species is considered as an intermediate derived from the adsorption and decomposition of N$_2$O on the surface of the catalyst. Here, NO was used as a probe molecule to detect the formation of the oxygen species on the surface of the Ru/Al$_2$O$_3$-NaBH$_4$ catalyst, which was pretreated by N$_2$O for 1 h at 300 °C. In Figure 11, NO was fed inside the cell; four intense peaks at 1628, 1523, 1411 and 1353 cm^{-1} were observed, which were related to nitrate and nitrite species. The peaks at 1411 and 1353 cm^{-1} were assigned to adsorbed monodentate nitrite [50]. Interestingly, two intense absorption bands at 1523 and 1628 cm^{-1} related to adsorbed NO$_2$ were observed [46,51]. This means that the O interacted with NO to become NO$_2$. In order to confirm that O was derived from N$_2$O or Al$_2$O$_3$, the DRIFTS of NO adsorption on Ru/Al$_2$O$_3$-NaBH$_4$ and Al$_2$O$_3$ catalysts, which were not pretreated by N$_2$O, are displayed in Figure S1 (Supporting Information). It can be seen that two intense absorption bands at 1523 and 1628 cm^{-1} were not observed for the b and c lines. Thus, it suggested that the Ru/Al$_2$O$_3$-NaBH$_4$ catalyst was pretreated by N$_2$O, resulting in the production of the new species α-O, which can interact with NO becoming NO$_2$ adsorbed on the surface of the catalyst. On the whole, this illustrates that the adsorbed N$_2$O species can be dissociated to the O atom adsorbed on the Ru species to form the α-O species, which was not desorbed.
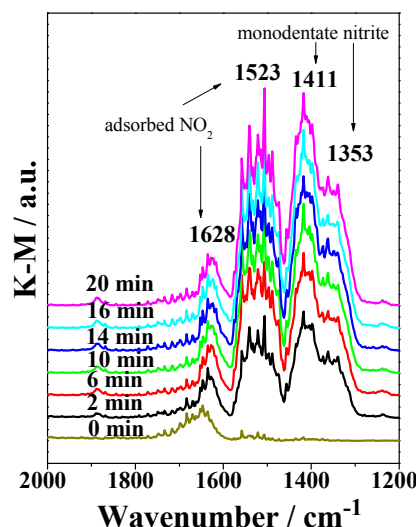
Figure 11. DRIFTS of Ru/Al$_2$O$_3$-NaBH$_4$ pretreated by 0.5% N$_2$O for 1 h at 300 °C, with exposure to NO (0.5% in He, 20 mL/min) at 300 °C. Condition: [N$_2$O] = 5000 ppm, [NO] = 5000 ppm.

The N$_2$O-TPD-MS was studied for Ru/Al$_2$O$_3$-NaBH$_4$, displayed in Figure 12. The additional MS signals, such as O$_2$, N$_2$ and N$_2$O, were also tracked for monitoring. It can be seen that a large amount of N$_2$O molecule gradually desorbed from 140 °C, and the peaks were observed at 164 °C, 370 °C and 425 °C. In addition, the peak of the N$_2$ molecule was observed at 227 °C accompanying the desorption of N$_2$O. Moreover, a small amount of O$_2$ was also observed at 300 °C. This suggested that the decomposition of partial N$_2$O occurred along with the desorption of N$_2$O.
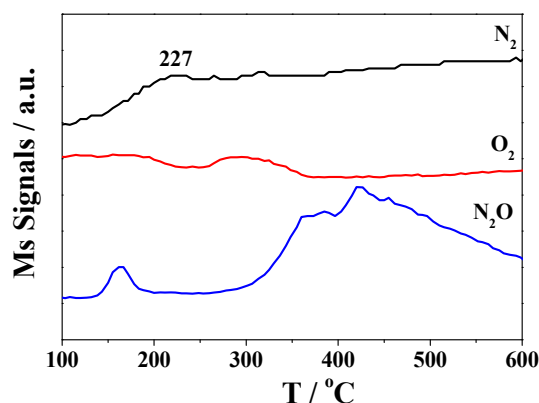
Figure 12. N$_2$O-TPD-MS profiles of Ru/Al$_2$O$_3$-NaBH$_4$. Detection signals: 28 (N$_2$), 32 (O$_2$) and 44 (N$_2$O).

To further understand the reaction of N$_2$O decomposition, a simulation experiment was conducted on the conditions of the dynamics by temperature programming and mass spectrometry monitoring online. The temperature programmed surface reaction with N$_2$O (N$_2$O-TPSR) was studied for the Ru/Al$_2$O$_3$-NaBH$_4$ catalyst. Figure 13 shows N$_2$, O$_2$ and N$_2$O signals in the MS. It can be seen that N$_2$O molecule gradually decomposed from 325 °C. The N$_2$ and O$_2$ peak was observed along with N$_2$O molecule decomposition. Additionally, the intensity of N$_2$ was higher than about 2 times that of O$_2$, and it is similar to the intensity of N$_2$O. Therefore, it confirms that the N$_2$ and O$_2$ were produced in N$_2$O decomposition.
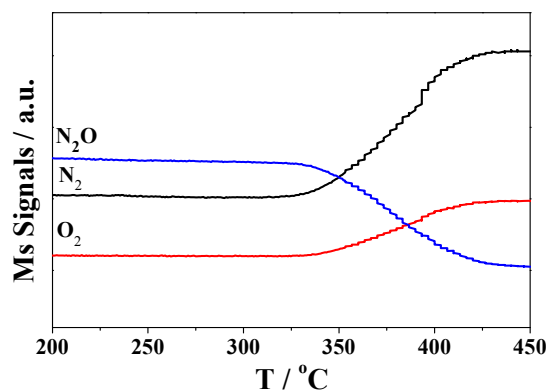
Figure 13. N_2O-TPSR profiles of Ru/Al_2O_3-$NaBH_4$. Detection signals: 28 (N_2), 32 (O_2) and 44 (N_2O).

3. Discussion

As shown in Figure 4, there were different catalytic activities among the Ru/Al_2O_3-H_2, Ru/Al_2O_3-$NaBH_4$ and Ru/Al_2O_3-air catalysts. In Figures 5 and 7, Ru/Al_2O_3 catalysts showed instable catalytic activity that decreased with the increase in times used, but the N_2O conversion was not affected at high temperatures. In Figure 2 (TEM), the Ru particle in the fresh Ru/Al_2O_3-$NaBH_4$ samples was not observed. This suggests that the particle size of Ru was small. However, the five-times used Ru/Al_2O_3-$NaBH_4$ catalyst showed agglomerates of Ru particles. The particles had an average size of about 5–20 nm, while particles with a size up to 40 nm could also be found. It was well known that the catalyst activity of metal is strongly dependent on the size. Therefore, the agglomeration of Ru particles was one of the deactivation reasons for the used Ru/Al_2O_3 catalysts. XPS results (Figure 3) confirmed the existence of the metallic Ru and Ru^{4+} species on the surface of the catalysts. The ratio of metallic Ru to Ru^{4+} was the difference on the surface of fresh and used catalysts and decreased with times used. From the relationship between the N_2O conversion and the amount of metallic Ru species (Figure 6), we think the metallic Ru plays a key role in conversion to N_2O. In addition, the effect of temperature is related to oxygen desorption, which also governs the deN_2O rate [52]. All catalysts display similar behavior, which may be due to the oxygen desorbed from RuO_2 promptly and Ru^{4+} going back to metallic Ru at high temperature. In order to verify the above idea, O_2-TPD-MS was studied for used Ru/Al_2O_3-$NaBH_4$, displayed in Figure 14. It can be seen that a large amount of O_2 molecule desorbed was observed between 100 °C and 250 °C, which was assigned to the desorption of adsorbed oxygen on Al_2O_3. However, desorption of the O_2 molecule in the range from 250 °C–450 °C was not found for used Ru/Al_2O_3-$NaBH_4$ catalyst. Therefore, oxygen desorbed from RuO_2 and Ru^{4+} transformed to metallic Ru was not taking place on the surface of the catalyst at high temperatures. In order to further understand the change of the Ru chemical state on the surface of Ru/Al_2O_3-$NaBH_4$ at high temperatures, the used Ru/Al_2O_3-$NaBH_4$ catalyst cooled under the atmosphere of He and was investigated by the XPS technique. Figure 15 presents the XPS and the peak fitting results of Ru3d for used Ru/Al_2O_3-$NaBH_4$ catalyst under He gas cooling. The peaks at 280.2 and 285.0 eV were attributed to the $3d_{5/2}$ of metallic Ru and Ru^{4+} species, respectively, and corresponding to the $3d_{3/2}$ binding energies at 284.4 (metallic Ru) and 289.1 eV (Ru^{4+}) [34,35]. The relative amounts of metallic Ru and Ru^{4+} species were calculated from the areas of the fitted Gaussian–Lorentzian components of Ru3d shown in Table 1. It was noteworthy that the amount of the metallic Ru was about 40% for used Ru/Al_2O_3-$NaBH_4$ under the He gas cooling, which was lower than that of fresh Ru/Al_2O_3-$NaBH_4$ (51%). The results reveal that the used Ru/Al_2O_3-$NaBH_4$ catalyst under the He gas cooling presents different Ru species (metallic Ru and Ru^{4+}), and the valence state of the Ru species increased after use. In addition, RuO_2 transforming to metallic Ru due to desorption of oxygen did not occur on the surface of the catalyst.
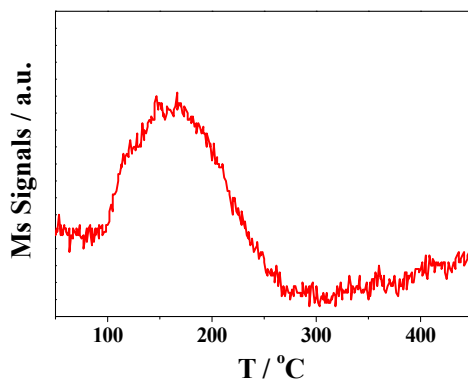
Figure 14. O_2-TPD-MS profiles of used Ru/Al_2O_3-$NaBH_4$. Detection signals: 32 (O_2).
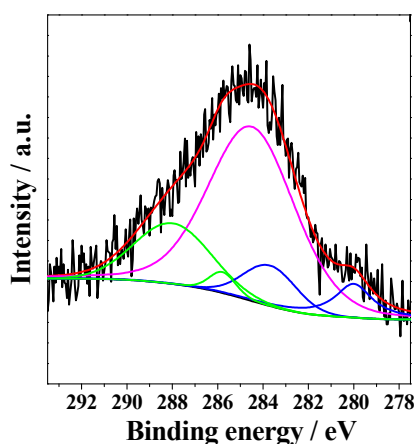
Figure 15. XPS of Ru3d for used Ru/Al_2O_3-$NaBH_4$ catalyst under the He gas cooling (black line: original data line; red line: fitting curve; pink line: the characteristic peak of C; blue line: the characteristic peak of metallic Ru; green line: the characteristic peak of Ru^{4+}).

Thus, the N_2O conversion of Ru/Al_2O_3 catalysts did not decrease at high temperature, which was mainly due to the high reaction rate, which was not the transformation of different species. Combining the above various characterization results, it is suggested that the metallic Ru is the active site. Following that, the reaction processes were brought out for Ru combined characterizations of DRIFTS, N_2O-TPD, TPRS, NO-TPD and XPS over Ru/Al_2O_3-$NaBH_4$.

In the DRIFTS of N_2O adsorption over Ru/Al_2O_3 (Figure 9), the species including chemisorbed N_2O and oxidized nitrogen species, like nitrites or nitrates, were observed. The oxidized nitrogen species were not reaction intermediates of N_2O decomposition, but they are just starters [44]. Ru was an active site; the nitrites, nitrates and nitro compounds were observed along with peaks characteristic for adsorbed N_2O (Figure 9b). The N_2O molecule adsorbed on the active center Ru through its O side to form the A-O_2N (Equation (1)). As reported in the literature [50,53], the HOMO of N_2O is a π-orbital associated with the O–N antibond and N–N bond, whereas the LUMO of N_2O is a π*-orbital with the antibonding character for both the O–N bond and N–N bond. A charge transfer occurs from HOMO of N_2O to Ru in the adsorption of N_2O. Meanwhile, the charge shift can also occur from the 4d of Ru to the LUMO of N_2O by the strong interaction with the feedback π bond, for which the charge transfers from the Ru to the middle N of N_2O [53]. Therefore, the first N_2O molecule adsorbs on the surface of the Ru catalyst to form A-ON_2 species, as demonstrated by the in situ DRIFTS experiments (Equation (1)).

Furthermore, the O–N bond of A-ON_2 species becomes greatly unstable and is easy to fracture and form A-O species and N_2 due to the strong interaction between Ru active sites and N_2O (Equation (1)).

From DRIFTS in Figure 11, it is proven that N_2O adsorbed on Ru/Al_2O_3-$NaBH_4$ can result in adsorbed oxygen species (A-O) on the surface of catalyst that is derived from the decomposition of A-ON_2 species (Equation (2)). Then, two active mono-oxygen species (A-O) diffuse on the surface of the catalyst and recombine into the gas-phase oxygen according to the Langmuir–Hinshelwood mechanism, and the whole catalytic cycle is closed (Equation (3)) [54,55]. On the other hand, A-O species also may react with another N_2O molecule by the Eley–Rideal mechanism. A-O, being a charge acceptor, interacts with the HOMO of another N_2O molecule as a charge donor to form O-A-ON_2 species on the surface of catalysts (Equation (4)) [56]. Meanwhile, the charges can also be transferred from the active site to the middle N of N_2O, resulting in facilitating the bond fracture of O–N_2, producing N_2 and bi-atomic oxygen species (O-A-O) (Equation (5)). The O-A-O species as the charge donors' intermediates can reorganize into another bi-atomic one (A-O_2), and then, O_2 can be desorbed from the A-O_2 by restoring of the active species (Equation (6)) [7,57–61].

In the DRIFTS of N_2O adsorption over Ru/Al_2O_3 (Figure 9), the band appearing at 1871 cm^{-1} was assigned to Ru–ON. This means the bond fracture of N–N producing Ru–ON and N after the N_2O molecule adsorbs on the surface of the Ru catalyst to form A-ON_2 species (Equation (7)). In the literature [62,63], the A–ON species was also captured by DRIFTS and DFT calculation; the reaction routes of N_2O decomposition are concluded as Equation (7). Then, two N diffuse on the surface of catalyst and recombine into the gas-phase N_2. In Figure 10a,b, the peak intensity of Ru–ON species became weak in the range of 250–375 °C. This suggests that the Ru–ON species was transformed or decomposed. Thus, the charges were transferred from the active site to the N of A-ON, resulting in facilitating the bond fracture of O–N producing A-O and N (Equation (8)). Then, two active mono-oxygen species (A-O) diffuse on the surface of the catalyst and recombine into the gas-phase oxygen according to the Langmuir–Hinshelwood mechanism, and the whole catalytic cycle is closed (Equation (9)) [55,56].

Moreover, XPS results indicate that the ratio of metallic Ru on the surface of catalyst decreases, and the Ru^{4+} amount presents the opposite change with increasing times used (Table 1). This is attributed to that part of the O species cannot desorb from the surface of catalysts, leading to the oxidation of metallic Ru to the high valence state of Ru species (Ru^{4+}). Thus, Equations (3), (6) and (9), which do not occur completely, will result in the increase in the oxidation state of Ru species.

The process can be described over Ru as follows:

$$N_2O \text{ (g)} + A \longleftrightarrow A\text{-}ON_2 \tag{1}$$

$$A\text{-}ON_2 \rightarrow A\text{-}O + N_2 \tag{2}$$

$$2A\text{-}O \rightarrow 2A + O_2 \tag{3}$$

$$A\text{-}O + N_2O \rightarrow O\text{-}A\text{-}ON_2 \tag{4}$$

$$O\text{-}A\text{-}ON_2 \rightarrow O\text{-}A\text{-}O + N_2 \tag{5}$$

$$O\text{-}A\text{-}O \rightarrow A + O_2 \tag{6}$$

$$A\text{-}ON_2 \rightarrow A\text{-}ON + N \tag{7}$$

$$A\text{-}ON \rightarrow A\text{-}O + N \tag{8}$$

$$2A\text{-}O \rightarrow 2A + O_2 \tag{9}$$
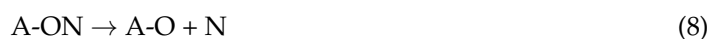
In summary, a linear relationship is displayed between the N_2O conversion and amount of metallic Ru. The decrease in the amount of metallic Ru on the surface of catalysts leads to the deactivation with increasing times used. From the characterization results, the deactivation reason can be attributed to the formation of Ru^{4+} species that is derived from the oxidation of the metallic Ru by oxygen species obtained in N_2O adsorption and decomposition. Additionally, agglomeration of Ru particles was another reason for deactivation.

4. Experimental Section

4.1. Materials

Ruthenium chloride (RuCl$_3$·xH$_2$O, 99.9%) was purchased from the Trace Elements Institute of Tongji University, Shanghai, China. Aluminum oxide (Al$_2$O$_3$) was purchased from Sinopharm Chemical Reagent Co., Ltd., Shanghai, China. Sodium borohydride was purchased from Aoran Fine Chemical Industry, Tianjin, China. Nitric oxide (NO, 99.9%), nitrous oxide (N$_2$O, 99.9%) and hydrogen (H$_2$, 99.999%) gases were purchased from Guangming Gas Chemical Industry Research Institute, Dalian, China. Helium (He, 99.999%) was purchased from Haipu Beifen Gas Industry Co., Ltd., Beijing, China. All chemicals were used as received without any further purification.

4.2. Catalyst Preparation

Ru/Al$_2$O$_3$-NaBH$_4$ was prepared as follows: Firstly, 10 mL RuCl$_3$·solution (5.00 mmol/L), 80 mL deionized water and 1.000 g commercial γ-Al$_2$O$_3$ were mixed under stirring at room temperature. Then, NaBH$_4$ (0.032 g) dissolved in 10 mL deionized water was dropwise added into the above mixture. The obtained mixture was stirred for 4 h at room temperature and then was filtered. The precipitate was washed with deionized water (about 1000 mL) till there was no chloride ion tested by AgNO$_3$ and dried at 110 °C overnight to obtain sample Ru/Al$_2$O$_3$-NaBH$_4$. Ru/Al$_2$O$_3$-H$_2$ and Ru/Al$_2$O$_3$-air were prepared according to the above process, except no addition of NaBH$_4$. The dry precipitate was calcined in air at 500 °C for 3 h to obtain sample Ru/Al$_2$O$_3$-air, while in pure H$_2$ at 300 °C for 1 h to get sample Ru/Al$_2$O$_3$-H$_2$.

4.3. Catalyst Characterization

The BET surface area of the samples was measured from the N$_2$ adsorption and desorption isotherms at −196 °C using a Micromeritics Tristar II 3020 analyzer. Ru content (wt %) was determined by inductive-coupled plasma-atomic emission spectroscopy (ICP-AES) (Optima 7000 DV, Perkin Elmer) (Perkin Elmer Limited, Waltham Mass, Waltham, MA, USA). The sample preparation for ICP-AES analysis was that certain samples were dissolved into the mixture of HF-HNO$_3$, which was made into a mixture concentration of 20–40 mg/L solution. X-ray diffraction (XRD) was performed by using a Bruker D8 Advance X-ray diffractometer with Cu Kα (λ = 1.5418 Å) radiation (40 kV, 40 mA). The diffraction patterns were scanned in the *2θ* range of 10-80° with steps of 0.02°. Transmission electron microscopy (TEM) measurements were taken on a JEM-2100 electron microscope (JEOL, Tokyo, Japan) operating at 200 kV. XPS was made on an AXIS ULTRA DLD X spectrometer (Kratos Analytical Limited, Kyoto, Japan) using Al Kα radiation as the excitation source. The analysis range was 300 × 700 nm. In addition to a survey spectrum, detailed scans of the Ru (3d) and C (1s) regions were acquired for each sample. N$_2$O-TPD-MS or TPSR was carried out by using the AutoChem TP5080 chemisorption analyzer (Xianquan, Tianjin, China) and mass spectra (QIC-20) online analysis (HIDEN, Warrington, UK). The signals with m/z equal to 28 (N$_2$), 32 (O$_2$) and 44 (N$_2$O) were monitored during the N$_2$O-TPD measurements. In the typical experiment, catalyst (0.100 g) was placed in a quartz reactor and preconditioned in flowing He (25 mL/min) for 1 h at 300 °C, followed by cooling to room temperature. Then, the sample was heated to 600 °C at a rate of 10 °C/min in N$_2$O to record the TPD spectra with MS, completing N$_2$O-TPSR. Another the sample was saturated with 0.5% N$_2$O at a flow rate of 25 mL/min for 1 h at atmospheric pressure. After, the sample was swept with He at a rate of 30 mL/min for 1 h in order to remove the residual N$_2$O. Finally, the sample was heated at a rate of 10 °C/min from 20 °C–850 °C under a He flow of 30 mL/min. In situ DRIFTS were recorded with a Nicolet 6700 spectrometer (Thermo Fisher Scientific, Waltham, MA, USA) with an in situ diffuse reflectance cell (Harrick) and high sensitivity Mercury Cadmium Telluride (MCT) detector, which was cooled by liquid N$_2$. The DRIFTS cell was fitted with ZnSe windows and a heating cartridge that allowed samples to be heated to below 450 °C. The catalyst was heated to 300 °C under N$_2$ flow of 40 mL/min for 60 min to remove adsorbed impurities and then cooled to 50 °C.

The background spectrum was collected under a N_2 atmosphere and was subtracted from the sample spectra. The spectra were collected at 50 °C in the presence of a gas N_2O or NO (pretreated by N_2O) flow of 20 mL/min. The DRIFTS cell (flowing N_2O) was heated to different temperatures, and the spectra were collected after getting 10 min of steady state. The DRIFTS were recorded by accumulating 32 scans with a resolution of 4 cm^{-1}. The total flow rate of the feeding gas was kept at 40 mL/min. The IR spectra are presented as obtained without smoothing.

4.4. Catalytic Activity Test

Direct decomposition of N_2O was performed with a fixed-bed quartz-glass reactor with a 6 mm-diameter quartz glass tube. Gaseous mixtures of 0.5% N_2O with He were fed to the catalyst bed. In each experiment, 0.100 g of catalyst (40–60 mesh) without dilution were set in the reactor by using quartz wool. The feed flow rate was equal to 25 mL/min. At each examined temperature, the reaction was carried out for 60 min before measurements. The catalytic activity was tested in a temperature range of 250–450 °C. After the temperature went down to room temperature, repetitive experiments were also tested in a temperature range of from 250 °C–450 °C according to the above process. The concentration measurements of reaction products and remaining N_2O at the reactor outlet were performed by gas chromatography (Beifen Analytical Limited, Beijing, China) equipped with a 5A molecular sieve and Porapak Q columns. The activity of N_2O decomposition was evaluated by the following equations:

$$X_{N_2O} = \frac{(X_{N_2O_{in}} - X_{N_2O_{out}})}{X_{N_2O_{in}}} \times 100\%$$

where X_{N_2O} is the conversion to N_2O; $X_{N_2O_{in}}$ is the concentration of N_2O measured before the reaction; $X_{N_2O_{out}}$ is the concentration of N_2O measured after the reaction.

5. Conclusions

In this study, the Ru/Al_2O_3 (Ru/Al_2O_3-H_2, Ru/Al_2O_3-$NaBH_4$, Ru/Al_2O_3-air) catalysts with different amounts of metallic Ru have been prepared by changing the preparation process. The order of N_2O conversion was followed as: Ru/Al_2O_3-H_2 > Ru/Al_2O_3-$NaBH_4$ > Ru/Al_2O_3-air. The catalytic activities of the Ru/Al_2O_3 catalysts decrease with the increase in times used. The N_2O conversion displays a linear relationship with the amount of metallic Ru. Combining various characterizations, we think that the metallic Ru is the active site in N_2O decomposition. In situ DRIFTS studies confirm the reaction process of N_2O decomposition in the metallic Ru site. In the adsorption and decomposition of N_2O, oxygen species are not desorbed from metallic Ru, leading to the formation of the high valence state of Ru species (Ru^{4+}), resulting in deactivation. Therefore, one of the deactivation reasons is attributed to the decrease in the amount of metallic Ru on the surface of the Ru/Al_2O_3 catalysts with increasing times used. It was also found that the size of Ru particles increased for used catalyst. Thus, agglomeration of Ru particles was another reason for the deactivation.

Author Contributions: Y.Z. proposed, planned and designed the experiments. C.S. performed the experimental works. C.S., F.Y., Z.Z., C.Z. and X.N. contributed to the data analysis. C.S. and Y.Z. wrote the manuscript. Y.Z. supervised the project. All authors discussed the results and approved on the manuscript.

Conflicts of Interest: The authors declare no conflict of interest.

References

1. Rodhe, H. A comparion of the contribution of various gases to the greenhouse effect. *Science* **1990**, *248*, 1217–1219. [CrossRef] [PubMed]

2. Parks, J.E. Less costly catalysts for controlling engine emissions. *Science* **2010**, *327*, 1584–1585. [CrossRef] [PubMed]

3. Kramlich, J.; Linak, W.P. Nitrous oxide behavior in the atmosphere, and in combustion and industrial systems. *Prog. Energy Combust. Sci.* **1994**, *20*, 149–202. [CrossRef]

4. Wang, J.; Ji, Y.; He, Z.; Crocker, M.; Dearth, M.; McCabe, R.W. A non–NH_3 pathway for NOx conversion in coupled LNT-SCR systems. *Appl. Catal. B* **2012**, *111*, 562–570. [CrossRef]

5. Perez-Ramirez, J.; Kapteijn, F.; Schoffel, K.; Moulijn, J.A. Formation and control of N_2O in nitric acid production: Where do we stand today? *Appl. Catal. B* **2003**, *44*, 117–151. [CrossRef]

6. Perez-Ramirez, J. Prospects of N_2O emission regulations in the European fertilizer industry. *Appl. Catal. B* **2007**, *70*, 31–35. [CrossRef]

7. Kondratenko, E.V.; Kondratenko, V.A.; Santiago, M.; Pérez-Ramírez, J. Mechanistic origin of the different activity of Rh-ZSM-5 and Fe-ZSM-5 in N_2O decomposition. *J. Catal.* **2008**, *256*, 248–258. [CrossRef]

8. Wang, J.; Xia, H.; Ju, X.; Feng, Z.; Fan, F.; Li, C. Influence of extra-framework Al on the structure of the active iron sites in Fe/ZSM-35. *J. Catal.* **2013**, *300*, 251–259. [CrossRef]

9. Konsolakis, M.; Drosou, C.; Yentekakis, I.V. Support mediated promotional effects of rare earth oxides (CeO_2 and La_2O_3) on N_2O decomposition and N_2O reduction by CO or C_3H_6 over Pt/Al_2O_3 structured catalysts. *Appl. Catal. B* **2012**, *123–124*, 405–413. [CrossRef]

10. Pietrogiacomi, D.; Campa, M.C.; Carbone, L.; Tuti, S.; Occhiuzzi, M. N_2O decomposition on CoO_x, CuO_x, FeO_x or MnO_x supported on ZrO_2: The effect of zirconia doping with sulfates or K^+ on catalytic activity. *Appl. Catal. B* **2016**, *187*, 218–227. [CrossRef]

11. Yu, H.; Tursun, M.; Wang, X.; Wu, X. $Pb_{0.04}Co$ catalyst for N_2O decomposition in presence of impurity gases. *Appl. Catal. B* **2016**, *185*, 110–118. [CrossRef]

12. Zabilskiy, M.; Djinović, P.; Tchernychova, E.; Tkachenko, O.P.; Kustov, L.M.; Pintar, A. Nanoshaped CuO/CeO_2 materials: Effect of the exposed ceria surfaces on catalytic activity in N_2O decomposition reaction. *ACS Catal.* **2015**, *5*, 5357–5365. [CrossRef]

13. Komvokis, V.G.; Marti, M.; Delimitis, A.; Vasalos, I.A.; Triantafyllidis, K.S. Catalytic decomposition of N_2O over highly active supported Ru nanoparticles ($\leq$3 nm) prepared by chemical reduction with ethylene glycol. *Appl. Catal. B* **2011**, *103*, 62–71. [CrossRef]

14. Benco, L. Compensation effect. A DFT study of the activation of N_2O over *M*-CHA (*M* = Fe^{2+}, Co^{2+}, RuO^{2+}, RuO^+). *J. Catal.* **2013**, *298*, 122–129. [CrossRef]

15. Liu, N.; Zhang, R.; Li, Y.; Chen, B. Local Electric Field Effect of TMI (Fe, Co, Cu)-BEA on N_2O Direct Dissociation. *J. Phys. Chem. C* **2014**, *118*, 10944–10956. [CrossRef]

16. Kaczmarczyk, J.; Zasada, F.; Janas, J.; Indyka, P.; Piskorz, W.; Kotarba, A.; Sojka, Z. Thermodynamic Stability, Redox Properties, and Reactivity of Mn_3O_4, Fe_3O_4, and Co_3O_4 Model Catalysts for N_2O Decomposition: Resolving the Origins of Steady Turnover. *ACS Catal.* **2016**, *6*, 1235–1246. [CrossRef]

17. Kim, B.; Li, Z.; Kay, B.D.; Dohnalek, Z.; Kim, Y.K. Unexpected Nondissociative Binding of N_2O on Oxygen Vacancies on a Rutile TiO_2 (110)-1 $\times$ 1. *J. Phys. Chem. C* **2012**, *116*, 1145–1150. [CrossRef]

18. Pachatouridou, E.; Papista, E.; Delimitis, A.; Vasiliades, M.A.; Efstathiou, A.M.; Amiridis, M.D.; Alexeev, O.S.; Bloom, D.; Marnellos, G.E.; Konsolakis, M.; et al. N_2O decomposition over ceria-promoted Ir/Al_2O_3 catalysts: The role of ceria. *Appl. Catal. B* **2016**, *187*, 259–268. [CrossRef]

19. Amrousse, R.; Tsutsumi, A. Novel Rh-substituted hexaaluminate catalysts for N_2O decomposition. *Catal. Sci. Technol.* **2016**, *6*, 438–441. [CrossRef]

20. Jisa, K.; Novakova, J.; Schwarze, M.; Vondrova, A.; Sklenak, S.; Sobalik, Z. Role of the Fe-zeolite structure and iron state in the N_2O decomposition: Comparison of Fe-FER, Fe-BEA, and Fe-MFI catalysts. *J. Catal.* **2009**, *262*, 27–34. [CrossRef]

21. Zhang, C.; Zhang, Z.; Sui, C.; Yuan, F.; Niu, X.; Zhu, Y. Catalytic Decomposition of N_2O over Co-Ti Oxide Catalysts: Interaction between Co and Ti Oxide. *ChemCatChem* **2016**, *8*, 2155–2164. [CrossRef]

22. Konsolakis, M. Recent Advances on Nitrous Oxide (N_2O) Decomposition over Non-Noble-Metal Oxide Catalysts: Catalytic Performance, Mechanistic Considerations, and Surface Chemistry Aspects. *ACS Catal.* **2015**, *5*, 6397–6421. [CrossRef]

23. Li, Y.; Armor, J.N. Catalytic decomposition of nitrous oxide on metal exchanged zeolites. *Appl. Catal. B* **1992**, *1*, L21–L29. [CrossRef]

24. Chang, Y.; McCarty, J.G.; Wachsman, E.D. Effect of ruthenium-loading on the catalytic activity of Ru-NaZSM-5 zeolites for nitrous oxide decomposition. *Appl. Catal. B* **1995**, *6*, 21–23. [CrossRef]

25. Pinna, F.; Scarpa, M.; Strukul, G.; Guglielminotti, E.; Boccuzzi, F.; Manzoli, M. Ru/ZrO_2 Catalysts: II. N_2O Adsorption and Decomposition. *J. Catal.* **2000**, *192*, 158–162. [CrossRef]

26. Marnellos, G.E.; Efthimiadis, E.A.; Vasalos, I.A. Effect of SO_2 and H_2O on the N_2O decomposition in the presence of O_2 over Ru/Al_2O_3. *Appl. Catal. B* **2003**, *46*, 523–539. [CrossRef]

27. Lin, Q.; Huang, Y.; Wang, Y.; Lin, L.; Liu, X.Y.; Lv, F.; Wang, A.; Li, W.C.; Zhang, T. RuO_2/rutile-TiO_2: A superior catalyst for N_2O decomposition. *J. Mater. Chem. A* **2014**, *2*, 5178–5181. [CrossRef]

28. Kawi, S.; Liu, S.Y.; Shen, S.C. Catalytic decomposition and reduction of N_2O on Ru/MCM-41 catalyst. *Catal. Today* **2001**, *68*, 237–244. [CrossRef]

29. Beyer, H.; Emmerich, J.; Chatziapostolou, K.; Koehler, K. Decomposition of nitrous oxide by rhodium catalysts: Effect of rhodium particle size and metal oxide support. *Appl. Catal. A* **2011**, *391*, 411–416. [CrossRef]

30. Zheng, J.; Meyer, S.; Köhler, K. Abatement of nitrous oxide by ruthenium catalysts: Influence of the support. *Appl. Catal. A* **2015**, *505*, 44–51. [CrossRef]

31. Komvokis, V.G.; Marnellos, G.E.; Vasalos, I.A.; Triantafyllidis, K.S. Effect of pretreatment and regeneration conditions of $Ru/\gamma-Al_2O_3$ catalysts for N_2O decomposition and/or reduction in O_2-rich atmospheres and in the presence of NO_X, SO_2 and H_2O. *Appl. Catal. B* **2009**, *89*, 627–634. [CrossRef]

32. Boissel, V.; Tahir, S.; Koh, C.A. Catalytic decomposition of N_2O over monolithic supported noble metal-transition metal oxides. *Appl. Catal. B* **2006**, *64*, 234–242. [CrossRef]

33. Chen, X.; Delgado, J.J.; Gatica, J.M.; Zerrad, S.; Cies, J.M.; Bernal, S. Preferential oxidation of CO in the presence of excess of hydrogen on Ru/Al_2O_3 catalyst: Promoting effect of ceria-terbia mixed oxide. *J. Catal.* **2013**, *299*, 272–283. [CrossRef]

34. Elmasides, C.; Kondarides, D.I.; Grunert, W.; Verykios, X.E. XPS and FTIR study of Ru/Al_2O_3 and Ru/TiO_2 catalysts: Reduction characteristics and interaction with a methane-oxygen mixture. *J. Phys. Chem. B* **1999**, *103*, 5227–5239. [CrossRef]

35. Sayan, S.; Suzer, S.; Uner, D.O. XPS and in-situ IR investigation of $RuSiO_2$ catalyst. *J. Mol. Strut.* **1997**, *410–411*, 111–114. [CrossRef]

36. Lin, J.; Li, L.; Pan, X.; Wang, X.; Cong, Y.; Zhang, T.; Zhu, S. Catalytic decomposition of propellant N_2O over Ir/Al_2O_3 catalyst. *AIChE J.* **2016**. [CrossRef]

37. Pirngruber, G.D.; Frunz, L.; Pieterse, J.A.Z. The synergy between Fe and Ru in N_2O decomposition over FeRu-FER catalysts: A mechanistic explanation. *J. Catal.* **2006**, *243*, 340–349. [CrossRef]

38. Carl, P.J.; Larsen, S.C. Characterization of ruthenium-exchanged zeolites (beta, Y, and ZSM-5) by EPR spectroscopy. *J. Catal.* **2000**, *196*, 352–361. [CrossRef]

39. Esclapez, S.P.; Illán-Gómez, M.J.; Lecea, C.S.; Bueno-López, A. On the importance of the catalyst redox properties in the N_2O decomposition over alumina and ceria supported Rh, Pd and Pt. *Appl. Catal. B* **2010**, *96*, 370–378. [CrossRef]

40. Hussain, M.; Fino, D.; Russo, N. N_2O decomposition by mesoporous silica supported Rh catalysts. *J. Hazard. Mater.* **2012**, *211–212*, 255–265. [CrossRef] [PubMed]

41. Hadjiivanov, K.I. Identification of neutral and charged NxOy surface species by IR spectroscopy. *Catal. Rev. Sci. Eng.* **2000**, *42*, 71–144. [CrossRef]

42. Oktar, N.; Mitome, J.; Holmgreen, E.M.; Ozkan, U.S. Catalytic reduction of N_2O and NO_2 with methane over sol–gel palladium-based catalysts. *J. Mol. Catal. A* **2006**, *259*, 171–182. [CrossRef]

43. Wang, Y.; Lei, Z.; Chen, B.; Guo, Q.; Liu, N. Adsorption of NO and N_2O on Fe-BEA and H-BEA zeolites. *Appl. Surf. Sci.* **2010**, *256*, 4042–4047. [CrossRef]

44. Haq, S.; Hodgson, A. N_2O adsorption and reaction at Pd (110). *Surf. Sci.* **2000**, *463*, 1–10. [CrossRef]

45. Parres-Esclapez, S.; Such-Basanez, I.; Illan-Gomez, M.J.; Lecea, C.S.; Bueno-Lopez, A. Study by isotopic gases and in situ spectroscopies (DRIFTS, XPS and Raman) of the N_2O decomposition mechanism on Rh/CeO_2 and Rh/γ-Al_2O_3 catalysts. *J. Catal.* **2010**, *276*, 390–401. [CrossRef]

46. Kondarides, D.I.; Chafik, T.; Verykios, X.E. Catalytic Reduction of NO by CO over Rhodium Catalysts: 2. Effect of Oxygen on the Nature, Population, and Reactivity of Surface Species Formed under Reaction Conditions. *J. Catal.* **2000**, *191*, 147–164. [CrossRef]

47. Matsouka, V.; Konsolakis, M.; Lambert, R.M.; Yentekakis, I.V. In situ DRIFTS study of the effect of structure (CeO_2–La_2O_3) and surface (Na) modifiers on the catalytic and surface behaviour of Pt/γ-Al_2O_3 catalyst under simulated exhaust conditions. *Appl. Catal. B* **2008**, *84*, 715–722. [CrossRef]

48. Karakas, G.; Mitome-Watson, J.; Ozkan, U.S. In situ DRIFTS characterization of wet-impregnated and sol–gel Pd/TiO_2 for NO reduction with CH_4. *Catal. Commun.* **2002**, *3*, 199–206. [CrossRef]

49. Baidya, T.; Bera, P.; Mukri, B.D.; Parida, S.K.; Kroher, O.; Elsener, M.; Hegde, M.S. DRIFTS studies on CO and NO adsorption and NO + CO reaction over Pd^{2+}-substituted CeO_2 and $Ce_{0.75}Sn_{0.25}O_2$ catalysts. *J. Catal.* **2013**, *303*, 117–129. [CrossRef]

50. Delabie, A.; Vinckier, C.; Flock, M.; Pierloot, K. Evaluating the activation barriers for transition metal N_2O reactions. *J. Phys. Chem. A* **2001**, *105*, 5479–5485. [CrossRef]

51. Miller, D.D.; Chuang, S.S.C. The effect of O_2 on the NO-CO reaction over Ag-Pd/Al_2O_3: An in situ infrared study. *Catal. Commun.* **2009**, *10*, 1313–1318. [CrossRef]

52. Kapteijn, F. Rodriguez-Mirasol, J. Moulijn, J.A. Heterogeneous catalytic decomposition of nitrous oxide. *Appl. Catal. B* **1996**, *9*, 25–64. [CrossRef]

53. Liu, N.; Chen, B.; Li, Y.; Zhang, R.; Liang, X.; Li, Y.; Lei, Z. Charge Transfer Analysis on the Direct Decomposition of Nitrous Oxide over Fe-BEA Zeolite: An Experimental and Density Functional Study. *J. Phys. Chem. C* **2011**, *115*, 12883–12890. [CrossRef]

54. Pérez-Ramírez, J.; Kapteijn, F.; Mul, G.; Moulijn, J.A. NO-assisted N_2O decomposition over Fe-based catalysts: Effects of gas-phase composition and catalyst constitution. *J. Catal.* **2002**, *208*, 211–223. [CrossRef]

55. Kapteijn, F.; Marban, G.; Rodriguez-Mirasol, J.; Moulijn, J.A. Kinetic analysis of the decomposition of nitrous oxide over ZSM-5 catalysts. *J. Catal.* **1997**, *167*, 256–265. [CrossRef]

56. Lavrov, V.V.; Blagojevic, V.; Koyanagi, G.K.; Orlova, G.; Bohme, D.K. Gas-phase oxidation and nitration of first-, second-, and third-row atomic cations in reactions with nitrous oxide: Periodicities in reactivity. *J. Phys. Chem. A* **2004**, *108*, 5610–5624. [CrossRef]

57. Fu, C.M.; Korchak, V.N.; Hall, W.K. Decomposition of nitrous oxide on FeY zeolite. *J. Catal.* **1981**, *68*, 166–171. [CrossRef]

58. Wood, B.R.; Reimer, J.A.; Bell, A.T.; Janicke, M.T.; Ott, K.C. Nitrous oxide decomposition and surface oxygen formation on Fe-ZSM-5. *J. Catal.* **2004**, *224*, 148–155. [CrossRef]

59. Heyden, A.; Keil, F.J.; Peters, B.; Bell, A.T. Comprehensive DFT study of nitrous oxide decomposition over Fe-ZSM-5. *J. Phys. Chem. B* **2005**, *109*, 1857–1873. [CrossRef] [PubMed]

60. Kondratenko, E.V.; Pérez-Ramírez, J. Mechanis and kinetics of direct N_2O decomposition over Fe-MFI zeolites with different iron speciation from temporal analysis of products. *J. Phys. Chem. B* **2006**, *110*, 22586–22595. [CrossRef] [PubMed]

61. Ryder, J.A.; Chakraborty, A.K.; Bell, A.T. Density functional theory study of benzene oxidation over Fe-ZSM-5. *J. Catal.* **2003**, *220*, 84–91. [CrossRef]

62. Chen, B.; Liu, N.; Liu, X.; Zhang, R.; Li, Y.; Li, Y.; Sun, X. Study on the direct decomposition of nitrous oxide over Fe-beta zeolites: From experiment to theory. *Catal. Today* **2011**, *175*, 245–255. [CrossRef]

63. Zhang, X.; Shen, Q.; He, C.; Ma, C.; Cheng, J.; Li, L.; Hao, Z. Investigation of Selective Catalytic Reduction of N_2O by NH_3 over an Fe-Mordenite Catalyst: Reaction Mechanism and O_2 Effect. *ACS Catal.* **2012**, *2*, 512–520. [CrossRef]